

Spatial-Aware Dictionary Learning for Hyperspectral Image Classification

Ali Soltani-Farani, Hamid R. Rabiee, *Senior Member, IEEE*, Seyed Abbas Hosseini

Abstract—This paper presents a structured dictionary-based model for hyperspectral data that incorporates both spectral and contextual characteristics of a spectral sample, with the goal of hyperspectral image classification. The idea is to partition the pixels of a hyperspectral image into a number of spatial neighborhoods called contextual groups and to model each pixel with a linear combination of a few dictionary elements learned from the data. Since pixels inside a contextual group are often made up of the same materials, their linear combinations are constrained to use common elements from the dictionary. To this end, dictionary learning is carried out with a joint sparse regularizer to induce a common sparsity pattern in the sparse coefficients of each contextual group. The sparse coefficients are then used for classification using a linear SVM. Experimental results on a number of real hyperspectral images confirm the effectiveness of the proposed representation for hyperspectral image classification. Moreover, experiments with simulated multispectral data show that the proposed model is capable of finding representations that may effectively be used for classification of multispectral-resolution samples.

Index Terms—Classification, hyperspectral imagery, dictionary learning, probabilistic joint sparse model, linear support vector machines.

I. INTRODUCTION

NATURAL SIGNALS are primarily modeled as members of a vector space. The dimensionality of this space is usually much higher than the number of underlying causes. This is mainly due to the inherent limitations of natural and artificial sensors, which often neglect the underlying causes of real world phenomena and therefore sample data at rates far exceeding the effective dimension of the signals. Learning these causes and thus representing a signal in a low-dimensional model is the goal of a recent trend of research known as dictionary learning [1]–[3]. The idea is to represent a signal by a linear combination of a few elements from a dictionary that is learned from the data. Each data point is thus represented through a sparse vector of coefficients, as a member of a low-dimensional subspace spanned by a few dictionary elements. When the dictionary is fixed this process is commonly known as sparse coding. Dictionary learning has achieved great success in signal reconstruction tasks such as compression [4] and denoising [5]. More recently, it has also been applied to discriminative tasks such as classification [6]–[10] and clustering [11], [12] with state-of-the-art results.

A hyperspectral image is a collection of pixels that represent a given scene or object, where pixels represent the reflected so-

lar radiation from the Earth’s surface in many narrow spectral bands [13]. At each pixel, the spectral features form a vector whose elements correspond to the narrow bands covering visible to infrared regions of the spectrum. The wealth of data provided by hyperspectral imagery (HSI) has promoted its application in many domains such as agriculture [14], [15], defense [16], [17], and environmental management [18], [19]. The reflectance spectra of a pixel are influenced by a number of factors. Apart from measurement noise caused by variation in illumination and viewing angle, and environmental effects such as aerosols and moisture, the spectral features of a pixel are determined by the material present at the given pixel and its surrounding area. Due to the spatial resolution of the imaging device, scattering from the local scene, and material mixtures within a pixel, each pixel is often composed of a number of different materials plus noise [20], [21]. Spectral unmixing is the process of identifying the pure materials present in the mixture, called *endmembers* and their respective *abundances*. The linear mixture model (LMM) which is commonly used for unmixing assumes that each pixel, x is composed of a linear combination of endmembers, $D = [d_1, \dots, d_K]$ plus an additive noise, ϵ , i.e.

$$x = Dy + \epsilon \quad (1)$$

where the fractional abundances, y are commonly assumed to be nonnegative and sum to unity. This is essentially the idea encouraged by dictionary learning with one difference, that in dictionary learning the fractional abundances are mainly assumed to be sparse. The aim of dictionary learning is to reduce the error in representing each signal while inducing sparsity in the representation coefficients. This is commonly accomplished through a formulation such as:

$$\arg \min_{D, y_i \in \mathcal{C}} \sum_{i=1}^N \left(\frac{1}{2} \|x_i - Dy_i\|_2^2 + \gamma \mathcal{S}(y_i) \right) \quad (2)$$

where N is the number of signals available for training, $\mathcal{S}(y)$ is a sparsity inducing regularizer such as the well known ℓ_1 norm, γ is a regularization parameter balancing representation error with representation complexity, and \mathcal{C} represents constraints on the sparse coefficients.

Recently, inspired by the ability of dictionary learning to model high-dimensional data and its potential to learn high-level information from the training samples [1], [3], sparse coding and dictionary learning have been used for spectral unmixing with encouraging results. The sparse unmixing approach proposed in [22] assumes that a set of pure spectral signatures are available which compose the dictionary. The

Manuscript received March 18, 2013; revised July X, 2013. This work was supported in part by the AICT Research Center.

A. Soltani-Farani, H. R. Rabiee, and S. A. Hosseini are with the Department of Computer Engineering, Sharif University of Technology, Tehran, Iran.

fractional abundances are estimated using sparse coding with an ℓ_1 regularizer, taking into account the fact that a few number of endmembers contribute to a given pixel. This approach was later extended in [23], where it is assumed that all pixels in an image have fractional abundances with a common sparsity pattern. This is achieved by using a joint sparse regularizer to also decrease the total number of endmembers activated for an image. Since spectral libraries are often composed of groups of spectral signatures, [24] proposes a group Lasso formulation to exploit this fact. Motivated by the observation that pixels in a hyperspectral image are usually surrounded by similar pixels, [25] include the total variation (TV) regularization in the sparse unmixing formulation to encourage smooth variation in the fractional abundance of each endmember among adjacent pixels. The aforementioned approaches assume a library of pure spectra is given a priori which make up the dictionary (i.e. D is fixed in (2)). Selecting endmembers from the data has also been attempted both manually, based on the similarity between eigenvectors of the scene and the data [26] or automatically, based on a measure of modeling quality [20]. In contrast, [27]–[29] attempt to learn the set of spectral endmembers using dictionary learning. In [27] the dictionary is learned from unsupervised training data by considering a probabilistic LMM framework, wherein the additive noise is assumed to be Gaussian and the fractional abundances are i.i.d. Laplacian and constrained to be nonnegative. Experimental results show that the learned dictionary elements are similar to the material spectra available in the scene and may be used to infer samples with HSI-resolution from multispectral-level measurements. The work of Greer [29] differs from [27] in that the dictionary is assumed to have full rank and the fractional abundances must sum to unity. Hence, the ℓ_1 sparsity regularizer used in previous work no longer applies. A recent survey of different approaches for hyperspectral unmixing is presented in [21].

The high spatial and spectral resolution of a hyperspectral image provides the potential for each pixel to be accurately and robustly labeled as one of a known set of classes. Hyperspectral image classification has been applied to both urban [30] and agricultural [31] scenery. Various methods have been developed for this application. Among them are supervised techniques such as maximum likelihood and Bayesian classifiers [32], decision trees [33], neural networks [34], and support vector machines (SVM) [35], [36]. Semisupervised learning based on graph construction [37] and transductive SVMs [38] have also been proposed which take advantage of both labeled and unlabeled samples for classification. Inspired by the fact that pixels in a hyperspectral image are often surrounded by pixels of the same class, recent methods have focused on both spectral and contextual characteristics of HSI. The composite-kernel SVM [39] makes use of Mercer's theorem to construct kernels composed from a spectral kernel and a contextual kernel. In particular, the weighted sum of the spectral and contextual kernels has been successful in classifying images with limited training samples. The graph kernel SVM [40] incorporates both spectral and contextual characteristics simultaneously into a recursive graph kernel, and is also effective for small training sample sizes. Due to its recent success in discriminative tasks with small training

data [6]–[12], dictionary learning and sparse coding have also been applied to hyperspectral image classification. A sparsity-based model is proposed in [41] where a test spectral sample joined with its surrounding pixels is represented by a few training samples from a fixed training dictionary. The test pixel is then labeled as the class whose training samples have the largest contribution in representing the pixel and its surrounding neighbors. Although the main focus of [27] is spectral unmixing, the authors demonstrate that using the fractional abundances instead of the raw spectral features improves the classification accuracy of the linear SVM for small training sets. In the approach proposed by Castrodad et al. [28], a dictionary is learned for each class of hyperspectral data in a supervised manner. For classification, the different dictionaries are concatenated to form a single dictionary. The sparse code (fractional abundance) corresponding to a new pixel is calculated using the sparse unmixing formulation accompanied by a spectral-spatial regularizer to enforce smooth variations in the sparse codes for neighboring pixels. The new pixel is then labeled as the class whose dictionary produces the lowest representation error and complexity.

The work discussed above for hyperspectral unmixing and classification enjoy a number of common and individual advantages and pose a number of remaining challenges which motivate our work. Specifically, we focus on a simple yet efficient approach to learn a dictionary for hyperspectral data that can incorporate contextual information, with the aim of hyperspectral image classification. Of the approaches for spectral unmixing, some assume that a set of pure spectral signatures are available which may compose the dictionary [22]–[25]. Chen et al. [41] use the complete set of training data as the dictionary, but with the aim of classification. Similar to [27]–[29] we learn a dictionary using the training data, which is less complex (i.e. consists of fewer atoms) yet is more effective for classification (Section IV). In terms of incorporating contextual information, as we discuss in Section III-A, [39]–[41] employ a window centered at the pixel of interest to gather contextual information. This hinders the potential for parallel computation [13] and the methods tend to use only contextual information. In fact, as we shall see in the experimental results of Section IV, SVM classification using the weighted sum of the spectral and contextual kernels [39] achieves highest accuracy when the spectral kernel is given zero weight. The methods of [40], [41] are also based on the contextual characteristics of HSI since the pixel and its surrounding neighbors are indistinguishable to the classifying process. Of the dictionary-based approaches, Iordache et al. [25] and Castrodad et al. [28] incorporate contextual information by augmenting (2) with a regularization term that enforces smooth variation in the sparse representation for neighboring pixels. In [25] the dictionary is fixed and [28] learns the dictionary without the proposed regularization term. This is perhaps in regard of the complex optimization procedure, which is in turn due to the fact that the sparse representations of different pixels can not be computed independent of each other. In contrast, we attempt to learn the dictionary and incorporate contextual information simultaneously, yet our optimization is simple and amenable to parallel computations.

In this paper, we propose a structured dictionary-based model for hyperspectral data that is impervious to the aforementioned issues and incorporates both spectral and contextual characteristics of a spectral sample into the sparse set of coefficients. The idea is to partition the pixels of a hyperspectral image into a number of spatial neighborhoods called contextual groups and to model each pixel with a linear combination of a few elements from a dictionary. Since pixels inside a contextual group are often made up of the same materials, their linear combinations are constrained to use common elements from the dictionary. Equivalently, they belong to the same subspace and their sparse coefficients have a common sparsity pattern. This is realized by using a joint sparsity inducing regularizer in the dictionary learning formulation of (2). We also show how this model may be viewed from a probabilistic perspective by building upon the basic probabilistic framework introduced in [3] and employed in [27]. Solving for the dictionary and sparse coefficients leads to a two-step optimization procedure that iterates between updating the dictionary and the sparse coefficients. Each step is a convex optimization which is well known in the literature and for which efficient solutions exist. Recent work in the field of computer vision using sparse coding and dictionary learning techniques [6]–[8] has shown that the extracted features therein are discriminative enough to be well classified using a simple classifier such as linear SVM. Motivated by these recent findings, we employ a linear SVM to classify the sparse representation corresponding to each pixel. Extensive experiments on real hyperspectral images are provided to assess the properties of the proposed model.

To summarize, we make the following main contributions: (i) We show that the proposed model is capable of incorporating both spectral and contextual characteristics of a spectral sample into the sparse set of coefficients. Extensive experiments on three hyperspectral datasets show that the inferred sparse coefficients are discriminative enough to be classified with state-of-the-art accuracy using a linear SVM. (ii) Charles *et al.* [27] show that the sparse coding model accompanied by an HSI dictionary can be used to infer HSI resolution data from simulated multispectral imagery (MSI). We classify the sparse representations retrieved from simulated MSI-resolution data and show that our model is capable of finding representations that may effectively be used for classification of MSI-level samples. (iii) Moreover, compared to dictionary-based hyperspectral image classification methods [28], [41], we use a smaller number of dictionary elements for classification and show that our method is amenable to efficient parallel processing.

The remainder of this paper is organized as follows. Section II provides the necessary background on dictionary learning and introduces the structured dictionary-based model for hyperspectral data. To gain further insight, the models are also analyzed from a probabilistic point of view. The details of both basic and structured models and their application to HSI classification is discussed in Section III. To demonstrate the effectiveness of the proposed model, extensive experimental results on several hyperspectral images are reported and analyzed in Section IV. Section V concludes this paper and discusses paths for future research.

II. DICTIONARY-BASED MODELS FOR HSI

In this section, we first provide a brief background on the general dictionary learning paradigm followed by a short analysis of the dictionary learning setting employed in [27], [28]. We then customize the general model into a structured joint-sparse model tailored for hyperspectral data. We also describe how learning the parameters of these models leads to convex programs for updating the dictionary and sparse representations. In the sequel, lower case and capital letters are used for vectors (x) and matrices (X) respectively. Random variables are written in boldface letters.

A. Dictionary learning: General Paradigm

Let $\mathcal{X} \subset \mathbb{R}^M$ denote the set of signals of interest, e.g. the pixels of a hyperspectral image. Given $x_1, \dots, x_N \in \mathcal{X}$, the fundamental goal of dictionary learning is to find a set of atomic signals $D = [d_1, \dots, d_K]$ that form the building blocks of \mathcal{X} , in the sense that any $x \in \mathcal{X}$ is represented by a linear combination of a few of these atoms, i.e.

$$x = Dy + \epsilon \quad (3)$$

where ϵ is a small residual due to modeling x in a linear manner with the sparse representation vector $y \in \mathbb{R}^K$. Depending on the particular application, the desired accuracy and complexity, and the nature of the signals, dictionary learning may take different forms, yet is often a regularized least squares optimization:

$$\arg \min_{D, Y} \frac{1}{2} \|X - DY\|_F^2 + \gamma \mathcal{S}(Y) \quad (4)$$

where $X = [x_1, \dots, x_N]$, $Y = [y_1, \dots, y_N]$, and $\|\cdot\|_F$ denotes the Frobenius norm of a matrix. The regularizer, $\mathcal{S}(Y)$ is mainly sparsity inducing but may also induce other forms of a priori knowledge and γ is the regularization parameter. The formulation of (4) may also be viewed from a probabilistic perspective. Assuming that the residual vectors are independent zero-mean Gaussians with covariance matrix $\sigma^2 I$ and using the Bayes rule, the posterior is given by:

$$P(D, Y|X) \propto P(X|D, Y)P(D)P(Y) \quad (5)$$

where $P(X|D, Y) = \prod_{i=1}^N \mathcal{N}(x_i|Dy_i, \sigma^2 I)$. For convenience, it is usually assumed that $P(D)$ is uniform, leaving $P(Y)$ as the only means of conveying one's knowledge about X . If D, Y are estimated from the *maximum a posteriori* or *MAP estimate* we arrive at a form similar to (4):

$$\arg \min_{D, Y} \frac{1}{2} \|X - DY\|_F^2 - \sigma^2 \log P(Y) \quad (6)$$

B. Dictionary Learning: Basic Setting

In its simplest form, dictionary learning is performed with an sparsity inducing regularizer that acts independently on y_1, \dots, y_N and also on the elements of these vectors, $y^{(1)}, \dots, y^{(K)}$. From a probabilistic perspective it is assumed that the sparse representations, y_1, \dots, y_N , are independent realizations of a random vector \mathbf{y} and that the elements of this random vector, $\mathbf{y}^{(1)}, \dots, \mathbf{y}^{(K)}$, are also independent

random variables distributed according to a common pdf, $P(y)$. Traditionally, a Laplacian distribution has been attractive as it leads to the well known Lasso or ℓ_1 minimization [44] for recovering Y :

$$\arg \min_{D, Y} \frac{1}{2} \|X - DY\|_F^2 + \gamma \sum_{i=1}^N \|y_i\|_1 \quad (7)$$

This is the form employed by [27], [28] for dictionary learning with the added constraint that all elements of D and Y are nonnegative. To avoid the trivial solution in which the rows of Y tend to zero while the dictionary atoms become prohibitively large, the above optimization is solved with the constraint that $\|d_i\| \leq 1$ for $i = 1, \dots, K$. This could have been accounted for in the prior, $P(D)$, as in [45], but would lead to slower training algorithms. Before discussing how the above optimization is solved, we briefly note that it was recently shown in [2] that realizations of the i.i.d. Laplacian are not sparse¹. This raises the question as to why solutions of ℓ_1 minimization are sparse and what prior distribution may be used to express sparsity. The authors show that the i.i.d. zero-mean Generalized Pareto Distribution (GPD):

$$P_{\text{GPD}}(y) = \frac{\lambda}{2} \left(1 + \frac{\lambda|y|}{q}\right)^{-(q+1)} \quad (8)$$

with order q and shape parameter $\frac{1}{\lambda}$ is a valid sparsity inducing prior for y , and the Lasso minimizes an upper bound on its MAP estimation. We are interested in this distribution because we later wish to generalize it to model the dependency between contextually related pixels. This will help us set the regularization parameter, γ in (2), so that contextual groups of different size are modeled with similar complexity (see Section II-C for more details). The above optimization is convex in either D or Y but not in both. A common two-step strategy is used for this problem. These steps are iterated until convergence.

1) *Sparse Coding*: In this step, D is fixed and the optimization is solved with regard to Y . The objective function in (7) is separable and may be solved for each y_i independently by:

$$\arg \min_{y_i} \frac{1}{2} \|x_i - Dy_i\|_2^2 + \gamma \|y_i\|_1 \quad (9)$$

which is known as the Lasso, BPDN, or ℓ_1 minimization. Several efficient algorithms have been proposed to solve (9) [46]–[48], among which we use the implementation of [47] provided by the SPAMS toolbox [49], [50].

2) *Dictionary Update*: For the dictionary update step, Y is fixed and the optimization becomes

$$\begin{aligned} \arg \min_D \quad & \frac{1}{2} \|X - DY\|_F^2 \\ \text{s.t. } \forall i \quad & \|d_i\|_2 \leq 1 \end{aligned} \quad (10)$$

which is quadratic in D . The gradient of the objective function equals $DYY^T - XY^T$ which is zero for $D = XY^T(YY^T)^{-1}$. To account for the constraints it suffices to project atoms with larger than unit norm onto the unit ℓ_2 ball. This is

¹To be accurate, realizations of the i.i.d. Laplacian do not exhibit a power law decay or equivalently are not compressible. See [2] for details.

the solution provided by [51], a straight forward approach which may suffer from calculating the inverse of YY^T . The method proposed in [48] solves the dual problem in an iterative manner and [3] employs a steepest descent strategy. An online dictionary learning algorithm is proposed in [49] which is suitable for problems with many training data. We use a Block Coordinate Descent (BCD) strategy that updates the dictionary atoms iteratively. Since the objective function is strongly convex, BCD is guaranteed to achieve the unique solution. The objective function for the j 'th atom may be written as $\frac{1}{2} \|R_j - d_j Y_T^j\|_F^2$, where Y_T^j is the j 'th row of Y in column form and $R_j = X - \sum_{i \neq j} d_i Y_T^i$. Keeping only the terms in d_j , a little algebra yields:

$$\begin{aligned} \arg \min_{d_j} \quad & \frac{1}{2} \left\| d_j - \frac{R_j Y_T^j}{\|Y_T^j\|_2^2} \right\|_2^2 \\ \text{s.t.} \quad & \|d_j\|_2 \leq 1 \end{aligned} \quad (11)$$

the solution of which is

$$d_j = \text{proj}_{\ell_2} \left(\frac{R_j Y_T^j}{\|Y_T^j\|_2^2} \right) \quad (12)$$

where $\text{proj}_{\ell_2}(x)$ denotes the projection of x in the unit ℓ_2 ball.

C. Dictionary Learning for HSI

In the dictionary learning formulation of (7), the sparse representations are assumed to be independent. This simplifies the sparse coding step of dictionary learning since the objective function becomes separable in y_1, \dots, y_N . In the case of HSI, this simple setting ignores the large spatial correlation of HSI pixels. To overcome this problem, we partition the pixels into a number of spatial neighborhoods called contextual groups. Pixels that belong to the same contextual group are often made up of the same material; accordingly we assume that their representations use a common set of atoms from the dictionary. Thus, the sparse representations of pixels that belong to the same group are no longer independent. In Section III-B we discuss how the contextual groups are defined. Let $\{\mathcal{G}_1, \dots, \mathcal{G}_g\}$, denote the set of contextual groups, defined as a partition on $\{x_1, \dots, x_N\}$, and $X_{\mathcal{G}_i} = [x_{i,1}, \dots, x_{i,|\mathcal{G}_i}|]$ represent the members of \mathcal{G}_i written as columns of the matrix $X_{\mathcal{G}_i}$. Accounting for the above assumption, the model in (3) may now be written as

$$X_{\mathcal{G}_i} = DY_{\mathcal{G}_i} + E_{\mathcal{G}_i} \quad (13)$$

where the columns of $Y_{\mathcal{G}_i}$ and $E_{\mathcal{G}_i}$ are respectively the sparse representations and error vectors corresponding to the spectral samples in the columns of $X_{\mathcal{G}_i}$. $Y_{\mathcal{G}_i}$ is a row sparse matrix i.e. its columns have a common sparsity pattern. To learn the dictionary and sparse representations, we employ the ℓ_2/ℓ_1 convex joint sparsity inducing regularizer in (4) to arrive at:

$$\begin{aligned} \arg \min_{D, Y} \quad & \frac{1}{2} \|X - DY\|_F^2 + \sum_{i=1}^g \gamma_{\mathcal{G}_i} \|Y_{\mathcal{G}_i}\|_{2,1} \\ \text{s.t. } \forall i \quad & \|d_i\|_2 \leq 1 \end{aligned} \quad (14)$$

where $\gamma_{\mathcal{G}_i}$ is the regularization parameter for the i th group and $\|Y\|_{2,1}$ is the ℓ_2/ℓ_1 norm defined as the sum of the ℓ_2 norms of the rows of Y .

From a probabilistic viewpoint, this is equivalent to assuming that Y_{G_1}, \dots, Y_{G_g} are independent realizations of a random matrix, Y_G , the rows of which are independent random vectors distributed according to a common pdf, $P(Y_{G,T})$. In other words, we consider the dependency between members of a contextual group, but similar to the setting in (7), we don't model the dependency between the dictionary atoms. To define $P(Y_{G,T})$, we propose to generalize the GPD for vector data as:

$$P(Y_{G,T}) = C_G \left(1 + \frac{\lambda_G \|Y_{G,T}\|_2}{q_G} \right)^{-(q_G+1)} \quad (15)$$

where C_G is the normalization factor, and $q_G > |\mathcal{G}| - 1$. We call this distribution ℓ_2 -GPD, since the ℓ_2 norm of the row $Y_{G,T}$, is distributed according to (8). This results in row-sparse matrices Y_G , which is equivalent to the above joint sparse model for each contextual group. Applying MAP estimation as before shows that (14) minimizes an upper bound on the MAP objective function with $\gamma_{G_i} = \sigma^2 \lambda_{G_i} (\frac{1}{q_{G_i}} + 1)$. we set $q_G = |\mathcal{G}|$ and use $\lambda_G = \sqrt{|\mathcal{G}|}$ to achieve similar sparsity in groups of different size. An interesting study, beyond the scope of our work, would be to include the representation complexity of each group in the model by inferring this parameter from the data. We should note that MAP estimation with a Laplacian prior on the ℓ_2 norm of each row of Y_G or an equivalent hierarchical prior as in [52] would also lead to (14) but suffers from the same issue discussed in Section II-B, i.e. its realizations are not row sparse matrices.

Similar to (7), the above optimization is convex in either D or Y , but not in both. We use the same two-step strategy of iterative sparse coding and dictionary update. Although, the dictionary update step need not be changed, the sparse coding phase can no longer be solved independently for each y_i . The objective function of this step is still separable and can be solved for each Y_G by:

$$\arg \min_{Y_G} \frac{1}{2} \|X_G - DY_G\|_F^2 + \gamma_G \|Y_G\|_{2,1} \quad (16)$$

where the columns of X_G are the spectral samples corresponding to the sparse representations in the columns of Y_G . This is the well known convex formulation of the joint sparse recovery [2] or simultaneous sparse approximation [43] problem, also known as the multiple measurement vector (MMV) [42] problem in the compressed sensing community. Other convex formulations for this problem follow the general ℓ_q/ℓ_p form with $q \geq 1$ and $p \leq 1$, among which ℓ_2/ℓ_1 and ℓ_∞/ℓ_1 formulations are more widely used. We adhere to the ℓ_2/ℓ_1 form for two reasons. First, the objective function of (16) is strongly convex for $|\mathcal{G}| > 1$, and therefore has a unique solution. Several algorithms exist that efficiently solve this problem [42], [53]–[55]. Second, we arrived at this formulation within a probabilistic framework by introducing the ℓ_2 -GPD prior of (15). The ℓ_2 norm in this formulation treats all entries of $Y_{G,T}$ equally while an ℓ_∞ norm is solely determined by the maximum absolute value in $Y_{G,T}$. In other words, the ℓ_2 norm treats all spectral samples alike, while the ℓ_∞ norm may bias Y_G towards using the dictionary atoms

for which a corresponding spectral sample with very high similarity exists.

Among the algorithms proposed to solve (16), Malioutov, et al. [53] show that the optimization may be posed as Second Order Cone Programming (SOCP) for which off-the-shelf optimizers are available. The inner loops of SOCP are computationally expensive and the algorithm is only suitable for small-size problems [53], [54]. The work of Lu, et al. [54] extends the Alternating Directions Method (ADM) of [56] to solve MMV recovery. Although the proposed algorithm is quite fast within an acceptable solution accuracy, there is no guarantee that each iteration of the algorithm will reduce the objective function. In fact, as is observed in [54] and explained by Yang et al. [56], if $X_G \neq DY_G$, the objective function may increase after some iterations. This is particularly important for our scenario of dictionary learning where a nonzero residual due to linear modeling is inevitable. We employ the regularized M-FOCUSS algorithm of Cotter et al. [42] which is simple, efficient, and also guaranteed to reduce the objective function in each iteration. The algorithm works by estimating the ℓ_2 norm of each row of Y_G , and then updating Y_G based on that estimate. Setting the gradient of the objective function in (16) to zero, we arrive at:

$$\Lambda D^T DY_G - \Lambda X_G^T D + \gamma_G Y_G = 0 \quad (17)$$

where $\Lambda = \text{diag}(\|Y_{G,T}^i\|_2)$. Using the Searle identity [57] suggests the following update equation

$$Y_G = \Lambda D^T (D \Lambda D^T + \gamma_G I)^{-1} X_G \quad (18)$$

where Λ is computed using the previous estimate of Y_G . The algorithm may be initialized from any random point for which $\forall i, \|Y_{G,T}^i\|_2 \neq 0$ and is terminated when the difference between consecutive estimates of Y_G is smaller than some threshold. Another solution for the optimization in (16) is based on a BCD strategy that iteratively solves (16) for each row of Y_G . This solution is derived similar to the BCD-based dictionary learning procedure explained in Section II-B2, hence for convenience we only provide the update rule for the j' th row of Y_G ,

$$Y_{G,T}^{j'} = \left(1 - \frac{\gamma_G}{\|R_j^T d_j\|_2} \right)_+ \frac{R_j^T d_j}{\|d_j\|_2^2} \quad (19)$$

in which $(x)_+ = \max(x, 0)$. Although applying (19) for each row is less expensive than applying (18), we have empirically found regularized M-FOCUSS to need far fewer iterations for convergence than the BCD-based algorithm.

III. DICTIONARY-BASED CLASSIFICATION OF HSI

In this section, we discuss how the models introduced in Section II are used for hyperspectral image classification. The basic idea is to learn a dictionary from the data and approximate each pixel with a linear combination of a few dictionary elements. The coefficients of this linear combination form a sparse vector that is used to classify the corresponding pixel. We briefly discuss how (7) is used in [27] to classify hyperspectral samples based on their spectral features. We then consider, as a basic extension, to learn the dictionary based on

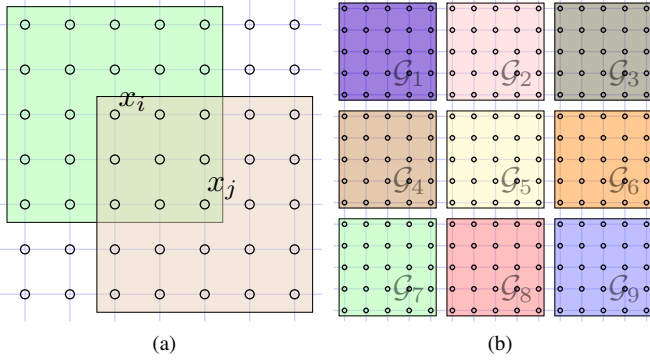


Fig. 1. (a) Block of a hyperspectral image. Shaded areas show windows centered at pixels x_i and x_j . The contextual representation of a pixel is computed from pixels inside its window. (b) Pixels of a hyperspectral image partitioned into 5×5 image patches, shown as shaded square regions.

contextual data alone. Finally, we explore how the structured model is learned from spectral data partitioned into predefined contextual groups.

A. Spectral/Contextual Dictionary Learning

To learn the dictionary D from spectral data, let x_1, \dots, x_N denote the spectral representation of the training data with respective labels l_1, \dots, l_N . Applying the dictionary learning formulation of (7) to these samples yields corresponding sparse representations y_1, \dots, y_N and the dictionary D . In [27] it is also assumed that the dictionary elements and sparse coefficients are nonnegative. A linear SVM is trained on the sparse representations and their corresponding labels l_1, \dots, l_N . Given a new spectral sample x , sparse coding is applied as in (9) to find the corresponding sparse representation y , which is then classified using the trained linear SVM to find the corresponding label l . This is a very straightforward method for applying dictionary learning to HSI classification. Like other classification methods that only make use of spectral characteristics of HSI, it has limited classification capability, which we shall observe in the experimental results of Section IV.

As was mentioned at the beginning of Section II-C, the basic dictionary learning model treats x_1, \dots, x_N independently and is unable to capture contextual information unless it is provided explicitly in the training data. To this end, let us define c_1, \dots, c_N as the contextual representation of the N training pixels with respective spectral representations x_1, \dots, x_N . Similar to [39], we define c_i as the moments computed separately over each spectral channel, from the samples surrounding x_i . Since the pixels surrounding x_i are often from the same class, this is similar to computing an estimate of the class moments local to x_i . Extracting the first moment in a local manner may also be viewed as applying a lowpass filter to the image in order to remove noise and derive features that are locally more alike. Also, as discussed in [32], the first and second moments of a class are particularly informative for HSI classification. Therefore, we set c_i to represent either the first moment or the concatenation of the first and second moments. Similar to [39]–[41], the surrounding pixels of x_i are

defined as those inside a square centered at x_i (See Fig. 1a) the width of which is determined by cross validation. Once more, applying the dictionary learning formulation of (7) with X replaced by $C = [c_1, \dots, c_N]$, results in corresponding sparse representations y_1, \dots, y_N and the dictionary D , which may be used to train a linear SVM. Given a new spectral sample x , we calculate its contextual representation c , and apply sparse coding to find the corresponding sparse representation y , which is again classified using the trained linear SVM. We shall refer to the basic dictionary model applied to contextual (spectral) data for HSI classification as contextual (spectral) dictionary learning.

B. Spectral-Contextual Dictionary Learning

Methods such as contextual dictionary learning, the composite kernel SVM of [39], and the joint sparsity model of [41] that use a window centered at the pixel of interest to calculate contextual information, have two important drawbacks. First, as is shown in Fig. 1a the windows that belong to neighboring pixels have large overlaps, which hinders the potential for parallel computation [13]. Second, these methods gain their classification power largely from contextual information. In the aforementioned contextual dictionary learning or Chen et al.'s joint sparse model [41], the spectral representation of the center pixel has as much significance in finding its label as any of the other pixels inside its window. Also, as we shall see in the experiments of Section IV, the weighted sum of spectral and contextual kernels [39] achieves highest accuracy when the weight of the spectral kernel is zero.

The advantages of dictionary learning for HSI data modeling as explained in Section I, together with the drawbacks of contextual-based methods as described above, and the limitations of the basic dictionary learning model, motivate the use of the structured dictionary learning model which can take advantage of both spectral and contextual information in HSI. To achieve this goal, we denote by x_1, \dots, x_N the spectral representation of the pixels in a hyperspectral image and define the contextual groups $\mathcal{G}_1, \dots, \mathcal{G}_g$, as non-overlapping image patches. Each patch is a $w \times w$ square of pixels². Fig. 1b shows how the pixels of a hyperspectral image may be partitioned into 5×5 squares of pixels. A number of other ways to define $\mathcal{G}_1, \dots, \mathcal{G}_g$ are imaginable. For example, HSI segmentation methods [13], [58] have a vast literature that may aid in defining more intelligent contextual groups that yield better results, yet we use the method illustrated in Fig. 1b for its simplicity and speed, and leave more complex methods to future research. In order to find the dictionary D and sparse representations y_1, \dots, y_N , we employ the dictionary learning formulation of (14). Once y_1, \dots, y_N are computed, we train a linear SVM on the sparse representation of the training data and classify the sparse representation of the test samples.

IV. EXPERIMENTAL RESULTS AND ANALYSIS

In this section, we provide experimental results to validate the effectiveness of the proposed structured dictionary-based

²If the image width or height are not divisible by w , at the bottom and right edges of the image the patches become smaller rectangles.

model for classifying real hyperspectral images. We compare the classification accuracies of the dictionary-based models, namely Spectral Dictionary Learning [27] (SDL), Contextual Dictionary Learning (CDL), and Spectral-Contextual Dictionary Learning (SCDL) with that of several methods. Support vector machines have proven successful in supervised classification of high-dimensional data such as HSI. Hence, we compare our results to SVM applied to spectral data with a polynomial kernel (SVM) [35], SVM applied to contextual data with an RBF kernel (CSVM) [39], and SVM with a weighted sum kernel from the composite kernel framework (CKSVM) [39]. Among the joint-sparsity-based HSI classification methods proposed recently in [41], the Simultaneous Orthogonal Matching Pursuit (SOMP) algorithm has achieved the best results, which we shall also use for comparison. We also compare the classification accuracy of SCDL with Dictionary Modeling with Spatial coherence (DMS) [28] and the graph kernel SVM (GKSVM) of [40] using the settings and results reported therein. In this section, methods that use contextual information collected from a window surrounding a pixel are further distinguished using μ for those that use the first moment, and μ, σ for those that employ both the first and second moments.

For the SVM-based approaches (SVM, CSVM, and CKSVM) all parameters (polynomial kernel degree d , RBF-kernel parameter σ , regularization parameter C , the composite kernel weight α , and the window width w) are obtained by five-fold cross validation. Table I shows the values that each variable was allowed to take in cross validation. For SOMP the same values of window size and sparsity level as those reported in [41] were used. The SOMP algorithm uses the ℓ_p norm to iteratively find the best atoms from the dictionary. At each iteration the correlation of all the signal residuals inside the window are found with each atom, and the atom for which the ℓ_p norm of the correlation vector is largest is chosen. As explained in [41], $p = 1, 2, \infty$ are most common. Unfortunately, the specific value of p used for each dataset is not given. Hence, we have tested each of the three values and reported the accuracy using the value of p that obtained the best results. For SOMP the complete set of training data was used as the dictionary. For SDL and CDL we also used five-fold cross validation to tune the parameters. The sparse regularization factor γ in (7) was allowed to take values from $\{0.1, 1, 10, 100\}$. To choose the number of dictionary atoms, values were chosen from $\{\frac{1}{2}, \frac{1}{4}, \frac{1}{8}, \frac{1}{16}\}$, as a fraction of the number of training data. The window size for CDL was also chosen from the same range as CSVM and CKSVM shown in Table I. For SCDL we use $\sigma^2 = 10$ for all datasets to obtain γ_g for each contextual group in (14). For the relatively small Aviris Indian Pines dataset with lower spatial resolution we used a random selection of $\frac{1}{2}$ training data to initialize the dictionary and an 8×8 patch size. For the relatively large ROSIS Urban datasets with high spatial resolution we used $\frac{1}{8}$ training data to initialize the dictionary and a larger 16×16 patch size.

Of the reported methods, some require an M -class SVM classification, be it linear or nonlinear. We use the one-against-one strategy for multi class classification using SVMs. That

TABLE I
RANGE OF VALUES USED IN CROSS VALIDATION FOR SVM, CSVM, AND CKSVM

Parameter	d	σ	C	α	w
Range	1:10	$10^{-1:3}$	$10^{-1:7}$	0 : 0.1 : 1	{3, 5, 7, 9}

TABLE II
INDIAN PINES GROUND-TRUTH CLASSES AND TRAIN/TEST SETS

Class		Samples	
No	Name	Train	Test
1	Alfalfa	6	48
2	Corn-notill	144	1290
3	Corn-min	84	750
4	Corn	24	210
5	Grass/Pasture	50	447
6	Grass/Trees	75	672
7	Grass/Pasture-mowed	3	23
8	Hay-windrowed	49	440
9	Oats	2	18
10	Soybeans-notill	97	871
11	Soybeans-min	247	2221
12	Soybean-clean	62	552
13	Wheat	22	190
14	Woods	130	1164
15	Building-Grass-Trees-Drives	38	342
16	Stone-steel Towers	10	85
Total		1043	9323

is, $\binom{M}{2}$ binary SVM classifiers are trained, one for each pair of classes. To classify a new test sample, it is applied to all classifiers and the label chosen by the majority of the classifiers is selected. For our experiments we used the LIBSVM [59] implementation³.

A. AVIRIS Indian Pines Dataset

One of the datasets that is often used for evaluating HSI classification is the Indian Pines image [60]. It was collected over an agricultural/forested area in NW Indiana using the AVIRIS sensor. The image is 145×145 pixels in size with a spatial resolution of 20 m/pixel and consists of 16 ground-truth classes. The spectral vectors consist of 220 bands across the spectral range 0.2 to 2.4 μm , of which 20 noisy bands (104-108, 150-163, 220) corresponding to the region of water absorption are removed. Fig. 2 shows a color composite image of the Indian Pines dataset along with the ground-truth. Around 10% of the data are randomly chosen for training and the remaining 90% are used for testing. The specific classes and the number of train and test data in each class are reported in Table II.

The different classification approaches are compared in Table III, where the classification accuracy for each class, overall accuracy (OA), average accuracy (AA), and the κ coefficient measure [61] are reported. The overall accuracy measures the ratio of correctly classified pixels to all test pixels, while the average accuracy is simply the average of the accuracies for each class. The κ coefficient is computed from different entries in the confusion matrix and is a robust measure of agreement that corrects for random classification. The results are averaged

³All code used for the experiments is available at <http://ssp.dml.ir/wp-content/uploads/2013/07/HSI.zip>

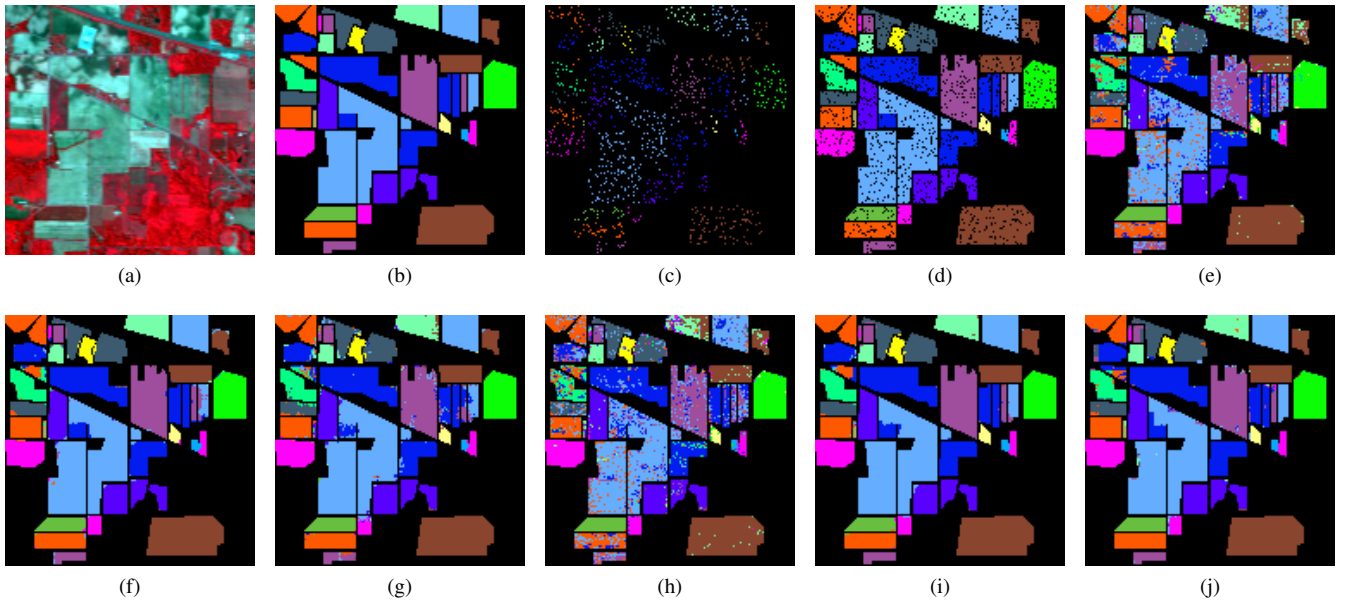


Fig. 2. Indian Pines image. (a) Three-band color composite (bands 50,27, and 17). (b) Ground-truth. (c) Training data. (d) Test data. Classification maps obtained by (e) SVM, (f) CSVM $_{\mu}$, (g) SOMP, (h) SDL, (i) CDL $_{\mu}$, and (j) SCDL colored according to Table II.

TABLE III
CLASSIFICATION ACCURACY (%) FOR AVIRIS INDIAN PINES FOR DIFFERENT CLASSIFIERS

Class	SVM	CSVM		CK SVM		SOMP	SDL	CDL		SCDL
	-	μ	μ, σ	μ	μ, σ	-	-	μ	μ, σ	-
1	74.37	81.67	92.29	81.88	87.08	89.79	61.04	96.88	96.67	93.75
2	79.17	96.33	96.51	96.02	95.82	93.73	76.04	98.02	98.15	94.93
3	70.92	96.84	96.79	96.44	97.12	92.18	68.85	97.57	97.49	97.39
4	72.00	94.57	92.10	93.33	92.05	94.10	56.19	96.67	96.52	90.57
5	93.29	95.28	96.67	95.48	96.17	92.89	91.54	97.85	97.52	97.23
6	95.40	98.54	98.17	98.66	98.71	98.99	95.31	99.55	99.24	99.17
7	75.65	67.39	74.35	69.13	79.57	55.65	43.04	87.39	87.39	100
8	97.95	98.20	98.80	98.27	98.95	99.89	98.95	99.98	100	99.95
9	64.44	62.22	78.89	57.78	81.11	3.33	16.67	61.11	58.33	79.44
10	66.15	95.13	96.33	93.83	94.88	87.46	64.11	97.09	97.11	96.30
11	81.70	97.45	97.58	97.39	97.36	97.46	82.50	98.89	98.78	98.46
12	77.63	95.83	95.83	95.63	95.85	87.57	73.48	96.76	96.90	92.97
13	99.21	98.42	98.37	98.84	98.26	98.53	99.05	98.32	98.26	99.05
14	94.18	98.33	98.55	97.90	97.72	98.63	95.29	99.81	99.63	98.87
15	61.78	94.97	94.65	93.83	93.45	97.40	58.04	98.10	99.04	97.13
16	91.29	90.47	87.29	93.53	92.47	92.94	90.12	93.41	96.47	96.00
OA	82.07 ± 0.68	96.63 ± 0.42	96.89 ± 0.36	96.34 ± 0.49	96.55 ± 0.42	94.73 ± 0.39	80.57 ± 1.02	98.28 ± 0.26	98.23 ± 0.22	97.18 ± 0.64
AA	80.95 ± 2.16	91.35 ± 2.06	93.32 ± 1.96	91.12 ± 1.90	93.54 ± 1.77	86.28 ± 1.95	73.14 ± 2.80	94.84 ± 1.53	94.78 ± 1.06	95.70 ± 2.12
κ	0.795 ± 0.008	0.961 ± 0.005	0.965 ± 0.004	0.958 ± 0.056	0.961 ± 0.048	0.940 ± 0.004	0.776 ± 0.009	0.980 ± 0.003	0.980 ± 0.003	0.968 ± 0.007

over ten runs and the standard deviation is also reported for OA, AA, and κ . The test and train data of the first run and the obtained classification map for each method is depicted in Fig. 2. There are a few observations to be made here. First, the methods based only on spectral characteristics (SVM and SDL) provide poor accuracies compared to the other methods that take into account contextual information. This stresses yet again the importance of contextual data for HSI classification. Second, the contextual kernel SVM (CSVM) provides marginally better results than the composite kernel SVM (CK SVM), which shows that CK SVM is unsuccessful in combining spectral and contextual characteristics of HSI. This is not very surprising considering the accuracies

reported for SVM and CSVM which yields the spectral kernel unlikely to contain complementary information. Third, the SOMP approach provides results comparable to CSVM for $p = \infty$, which means that the training data inside the window surrounding a pixel are always chosen as part of the best atoms, since each is both present in the window and the dictionary, and has maximum correlation with itself. This is somewhat similar to a k -nearest neighbor approach. This is also why the method obtains poor results for Oat pixels which cover a narrow region. As noted by Chen et. al [41], the local window for an Oat pixel is dominated by pixels from two adjacent classes. Fourth, since the Indian Pines map contains very large homogenous regions (Fig. 2b) there is little

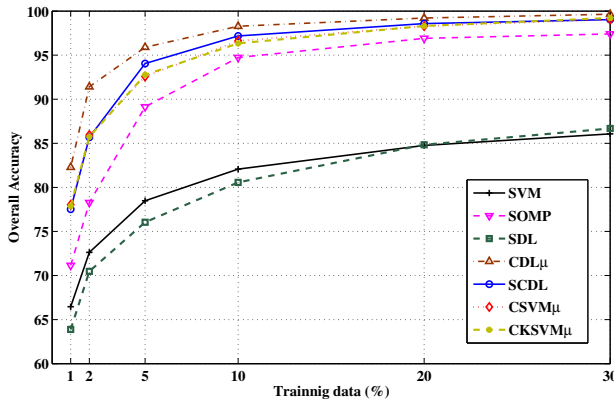


Fig. 3. Effect of number of training data on classification results for Indian Pines.

difference between using the first moment or using both the first and second moments inside a window as the contextual representation of a pixel. Finally, whilst CDL provides the best overall accuracy, its average accuracy is slightly lower than that of SCDL. This is due to the fact that SCDL is able to employ both spectral and contextual information, which puts CDL in a disadvantage when it comes to classifying classes with narrow regions (classes 7 and 9). SCDL provides high accuracies for each class but trails slightly behind CDL due to the mostly large homogenous regions present in the Indian Pines image. This shows that SCDL is likely to perform better than CDL for urban scenery where there are few large homogenous areas, as we see in the next section.

To further compare the different classification approaches reported in Table III, we have tested them on different training sample sizes. Fig. 3 shows the overall accuracy of each method for 1, 2, 5, 10, 20 and 30% training data averaged over ten runs. To avoid crowding the figure we have left out methods that use both the first and second moments since they have very similar results to the corresponding method that uses only the first moment. As the results show, CDL provides a large improvement for small number of training samples with SCDL trailing slightly behind. As was mentioned in Section I, dictionary learning has proven successful in classification problems where few training samples are available. As was expected, SOMP falls further behind as the number of training samples is decreased due to its similarity to a k -nearest neighbor approach.

For completeness, we also compare SCDL with the GKSVM [40] and DMS [28] using the same settings reported there. For 1% training data of the Indian Pines image, the authors reported 72.3% and 73.4% overall classification accuracy for GKSVM and DMS respectively. We obtained 76.2% using SCDL. For 5% training data the results reported in [28] are 83.5% and 84.4% for GKSVM and DMS respectively. Under this setting SCDL performs with 93.4% overall classification accuracy. For these experiments the GKSVM uses an 11×11 window centered at the pixels of interest to gather contextual information at two scales, while DMS encourages smooth variation in the sparse representations for

the four spatially connected neighbors, and as we mentioned earlier 8×8 contextual groups were employed for SCDL. Increasing the neighborhood size for DMS may increase the reported accuracy but would also incur a large increase in computational costs. It is also worth noting that the dictionary learned by SCDL has more than 50% less dictionary atoms than DMS. To be fair, we also performed experiments with a 3×3 patch size for SCDL leading to 72.6% and 87.9% overall accuracy for 1% and 5% training data respectively.

B. Dictionary Atoms and Sparse Representations

As a means of visual comparison, using 10% of the Indian Pines training data, we learned dictionaries with 138 atoms ($\frac{1}{8}$ th training data), using SDL, CDL $_{\mu}$, and SCDL. Fig. 4 depicts sample spectra for the classes Alfalfa, Wheat, Woods, and Stone-Steel Towers and the learned dictionary atom that is closest to each sample. An encouraging observation was that although we did not explicitly constrain neither the dictionary atoms nor the sparse representations to be nonnegative as in SDL, this was in fact almost always the case for CDL $_{\mu}$ and SCDL. The figure shows that all methods learn dictionary atoms that are quite similar to sample spectra obtained from the scene. This is inline with the observations made in [27]. CDL $_{\mu}$ seems to be more accurate in this regard, perhaps due to the denoising effect of spatial averaging. Since the dictionary atoms are similar to the sample spectra, the sparse representation of a sample with these atoms is likely to exhibit discriminative capabilities. To gain further insight, we have depicted in Fig. 5 and Fig. 6 the sparse representations obtained for an 8×8 contextual group, and also a line of 145 pixels in the Indian Pines dataset. From Fig. 5c one can see that a far fewer number of atoms are activated inside a contextual group for SCDL than for SDL (Fig. 5a) or CDL $_{\mu}$ (Fig. 5b). This was also observed in [23] where all samples in an image were grouped together to decrease the total number of atoms activated. In Fig. 6c one may observe that for almost every instance in a class of data a distinctive atom is active. This is sometimes violated at the edges of a class, where instances from different classes fall into the same contextual group. Although, the edges are where most misclassifications occur (see Fig. 2j and Fig. 9j), this is not always the case. The reason for this is that, while members of a contextual group are constrained to belong to the same subspace, they are not constrained to be any more similar within that subspace.

C. Classifying at MSI-Resolution Via HSI-resolution Atoms

A remarkable finding of [27] was that the sparse coding model accompanied by a dictionary learned from HSI-resolution data may be used to infer HSI-resolution spectra from simulated MSI-level measurements. Multispectral data generally have a much coarser spectral resolution (3-10 bands) than HSI data, and may be acquired in a more resource efficient manner. This motivates the need for processing at MSI-level with HSI-level quality. We follow the same experimental setting as [27] on the Indian Pines image, but since our goal is classification, we compare the overall classification accuracy

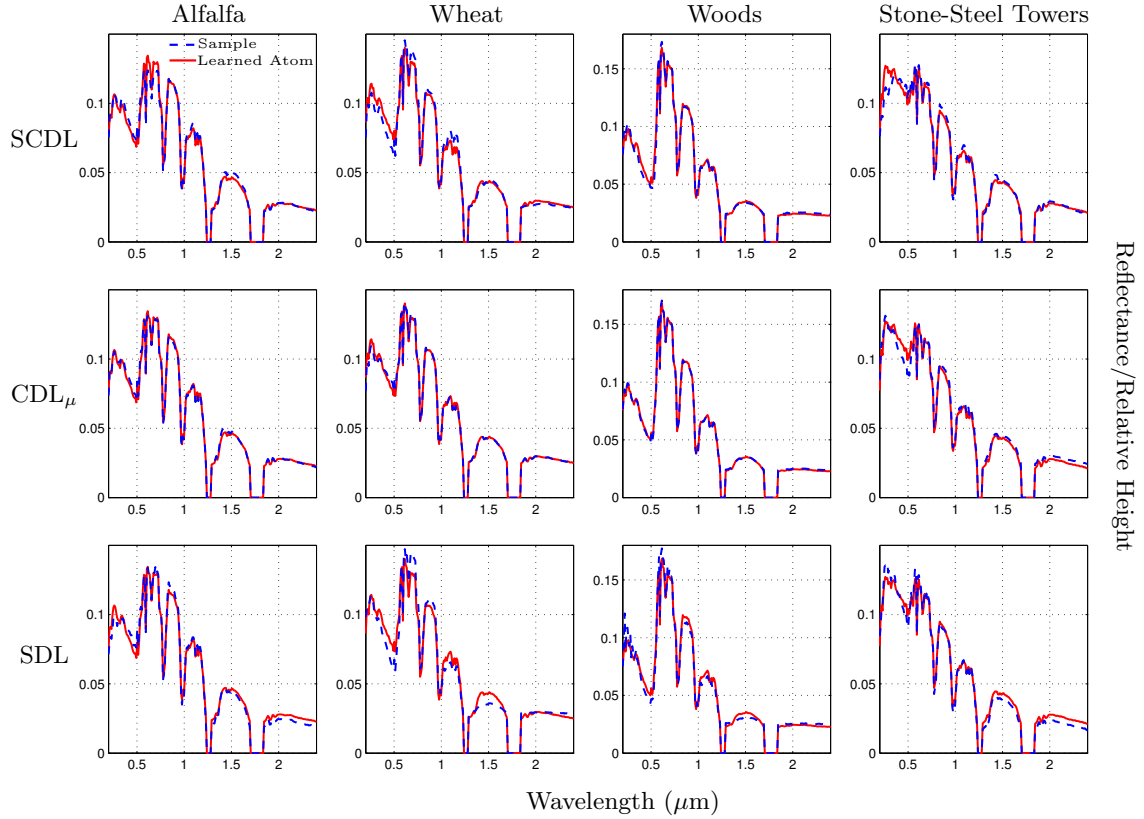


Fig. 4. Sample spectra for Alfalfa, Wheat, Woods, and Stone-Steel Towers in the Indian Pines dataset and the learned dictionary atom obtained by SDL, CDL, and SCDL that is closest to each sample. The two obvious gaps in the spectra correspond to the regions of water absorption which were removed.

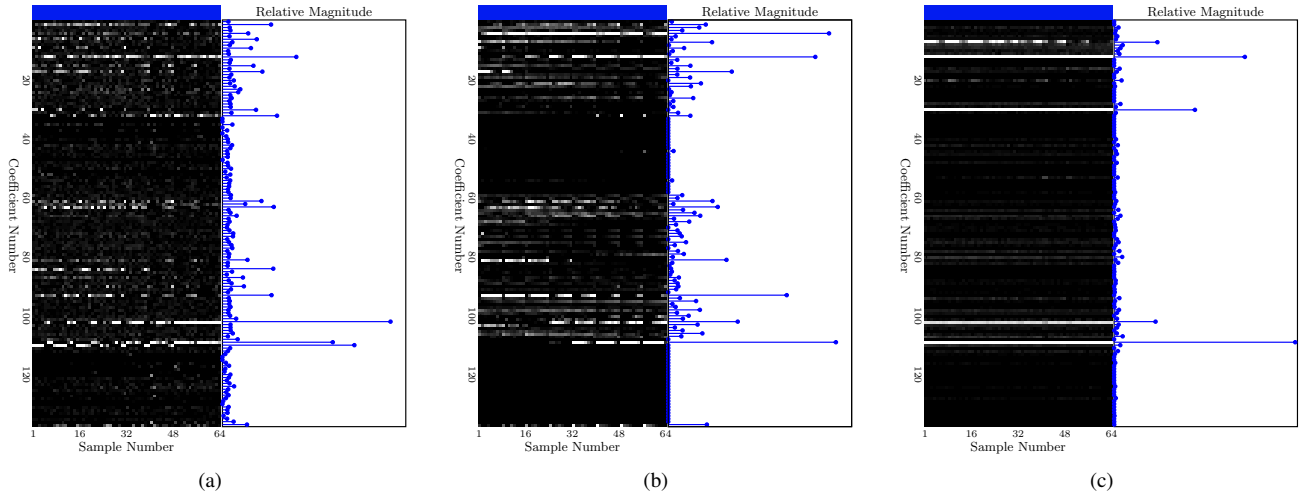


Fig. 5. Sparse coefficients corresponding to samples inside an 8×8 contextual group of the Indian Pines image accompanied on the right by the norm of each row of the coefficient matrix for (a) SDL, (b) CDL, and (c) SCDL. The label of each sample is shown above its coefficients.

using the retrieved sparse representations for SDL, CDL_μ , and SCDL.

To simulate MSI-level resolution spectra, it is assumed that each band is a linear combination of some adjacent spectral bands in the original HSI data. To be specific MSI-level data, $z \in \mathbb{R}^b$ are simulated from HSI spectra via $z = Bx$, where $B \in \mathbb{R}^{b \times N}$ ($b < N$) sums adjacent spectral bands of b non-overlapping bins in x . For one set of experiments $b = 8$ bins

are equally spaced in the lower half of the spectrum roughly corresponding to measurements obtained with the Worldview II MSI satellite [62] (MSI measurements), while for the second set of experiments, the $b = 8$ bins cover the complete spectrum (coarse HSI measurements).

Given a pre-learned HSI-resolution dictionary D , using (3) with the same line of arguments as in Sections II-B and II-C, we obtain the MAP estimate for the sparse representations of

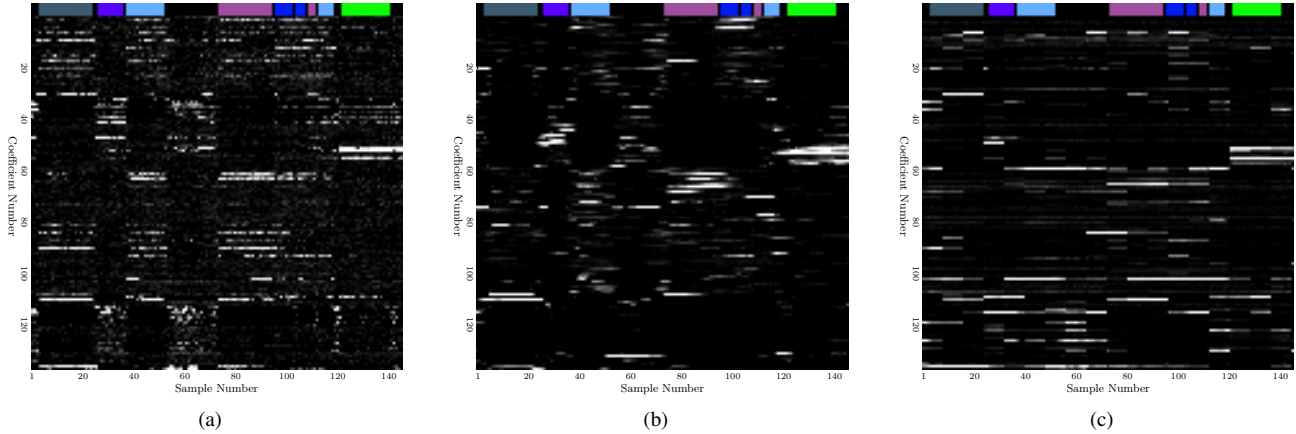


Fig. 6. Sparse coefficients corresponding to 145 samples on a horizontal line of the Indian Pines image for (a) SDL, (b) CDL, and (c) SCDL. The label of each sample is shown above its coefficients.

SDL/CDL and SCDL as:

$$\arg \min_Y \frac{1}{2} \|Z - BDY\|_F^2 + \gamma \sum_{i=1}^N \|y_i\|_1 \quad (20)$$

and

$$\arg \min_Y \frac{1}{2} \|Z - BDY\|_F^2 + \sum_{i=1}^g \gamma_{G_i} \|Y_{G_i}\|_{2,1} \quad (21)$$

respectively, where $Z = [z_1, \dots, z_N]$ are the MSI-resolution samples and Y are constrained to be nonnegative for SDL.

For each method, the samples are partitioned into initial train and test sets and the dictionary is learned. The test samples are then converted to MSI or coarse HSI (cHSI) measurements and again divided into test and train sets. After the sparse representations are obtained from (20) or (21), the train set is used to train a linear SVM and classification results are obtained for the test set. Fig. 7 shows the overall classification accuracy obtained for each method with 1, 2, 5, 10, 20, and 30% training data of the Indian Pines. The results show that all methods are able to obtain accuracies that are only slightly lower than those obtained with HSI-level measurements (Fig. 3). For CDL the results have decreased more significantly than SCDL. Considering the largely coherent columns of BD may explain this effect. As the columns of BD become more coherent, the sparse representations obtained by SDL or CDL exhibit larger spatial variations. This is not the case for SCDL which constrains pixels inside a contextual group to have a common sparsity pattern. We should note that these results serve as a proof of concept. In a more realistic scenario, the dictionary would be learned from a different but statistically similar scene, or from the same scene but at a different time.

D. Parallel Processing of Contextual Groups

In this section, we demonstrate how the computation cost of SCDL scales when contextual groups are processed in parallel with 1, 2 or 4 processing threads. We learned dictionaries initialized with $\frac{1}{2}$, $\frac{1}{4}$, and $\frac{1}{8}$ of the 10% training data of the Indian Pines dataset with an 8×8 patch size and $\sigma^2 = 10$. The dictionary learning algorithm was permitted to continue

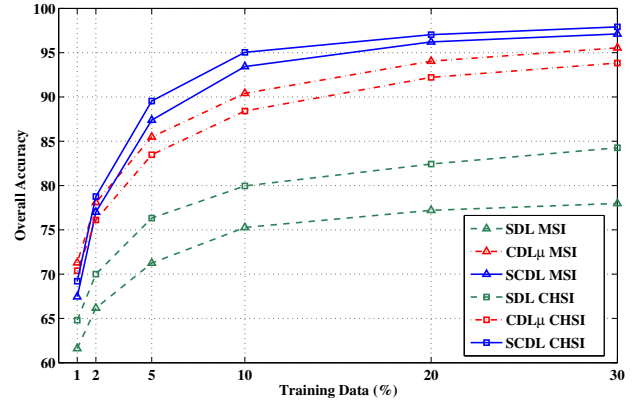


Fig. 7. Results for classification of the Indian Pines (synthetic) MSI and coarse HSI data using an HSI dictionary for different number of training data.

for 100 iterations and the overall classification accuracy was recorded after each iteration. Experiments were performed on a machine with an Intel Core i5-3570K 64 bit processor and 16 GBs of RAM. The code for M-FOCUSS was written in C++ and all timings were performed using MATLAB.

Fig. 8 shows the overall classification accuracy on this dataset as a function of time. A few observations may be made. First, since the dictionary is initialized with training data from the scene, one can see how consecutive iterations of the learning process affect the discriminative ability of the sparse codes. Although, since the learning process is unsupervised the classification accuracy is not always increasing, overall, dictionary learning increases the discriminative ability of the codes as it adapts to the statistics of the scene. Second, in terms of classification accuracy, the size of the dictionary seems to matter most in the early iterations, with only a 0.5% gap at the end for dictionaries initialized with $\frac{1}{8}$ and $\frac{1}{4}$ of the training data, and nearly no gap between $\frac{1}{4}$ and $\frac{1}{2}$. Third, the speedup gained from parallel processing is quite significant considering the different threads share the RAM. The first few iterations are often longer, while later iterations are shorter in

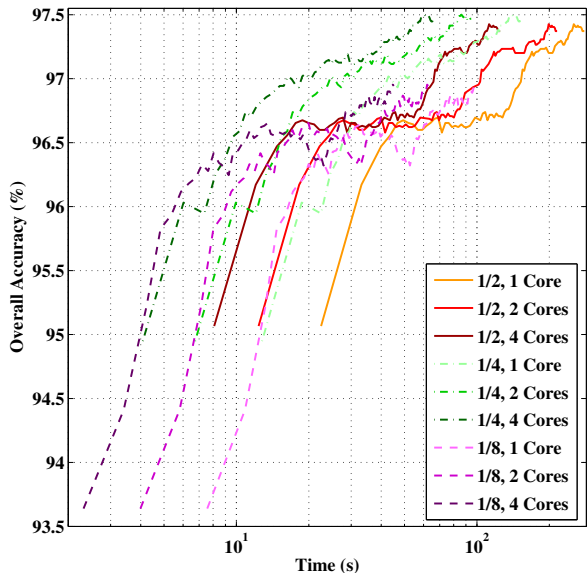


Fig. 8. Results for classification of the Indian Pines dataset with different dictionary size and different number of processing cores, as a function of time.

time and thus are more affected by time required for thread initialization. Also, the algorithm scales quite well with the dictionary size, considering the dictionary is shared between parallel jobs. The speed up was around 1.8 for 2 threads independent of dictionary size and was 3.3, 3.1, and 2.8 as dictionary size is increased when 4 threads were used.

E. ROSIS Urban Data over Pavia, Italy

ROSIIS urban data refers to two datasets, namely University of Pavia (Fig. 9), and Center of Pavia (Fig. 10), which were collected in 2003 by the ROSIS sensor with a spatial resolution of 1.3 m/pixel in 115 spectral bands covering 0.43 to 0.86 μm [13]. For both images, specific test and train sets are used for classification as in [13], [41], [58]. Fig. 9c and Fig. 10c show the training data for these images.

Table IV shows the 9 ground-truth classes and test and train sets of the University of Pavia image, which consists of 610×340 pixels in 103 spectral bands after 12 noisy bands were removed. Around 9% of the data are used for training, leaving 91% for testing. Experimental results for this image are reported in Table V with classification maps for most classifiers depicted in Fig. 9. Classification accuracies for this image are notably lower than the Indian Pines or Pavia Center images as is confirmed by [13], [41]. As noted earlier, SVM and SDL provide poor results since they only use the spectral characteristics. Unremarkably, CSVM and CKSVM provide the exact same results because the kernel weighting coefficient favors the contextual kernel in the cross-validation process of CKSVM. SOMP attains poor results because the training set is made up of small patches (Fig. 9c) and thus most likely the window surrounding a pixel contains no training samples. SCDL provides the best overall accuracy due to its ability to capture both spectral and contextual information. For

TABLE IV
UNIVERSITY OF PAVIA AND CENTER OF PAVIA GROUND-TRUTH CLASSES AND TRAIN/TEST SETS

University of Pavia				Center of Pavia			
Class		Samples		Class		Samples	
N	Name	Train	Test	N	Name	Train	Test
1	Asphalt	548	6404	1	Water	745	64533
2	Meadows	540	18146	2	Trees	785	5723
3	Gravel	392	1815	3	Meadow	797	2108
4	Trees	524	2912	4	Brick	485	1667
5	Metal sheets	265	1113	5	Soil	820	5729
6	Bare soil	532	4572	6	Asphalt	678	690
7	Bitumen	375	981	7	Bitumen	808	6479
8	Bricks	514	3364	8	Tile	223	2899
9	Shadows	231	795	9	Shadow	195	1970
Total		3921	40002	Total		5536	98015

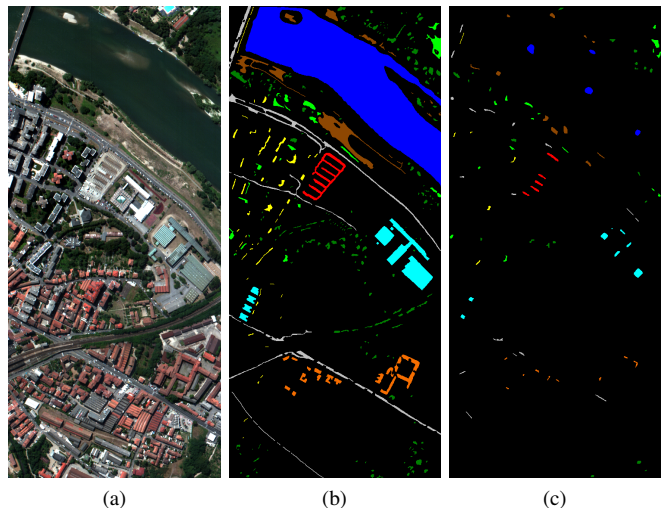


Fig. 10. Pavia Center image. (a) Three-band color composite (bands 50, 27, and 17). (b) Ground-truth (c) Train data colored according to Table IV.

further evaluation we chose random train and test data from the dataset and compared the overall classification accuracy of CSVM $_{\mu}$, SOMP, CDL $_{\mu}$, and SCDL. The results are found in Table VI where the average accuracy and standard deviation is reported for 10 runs. Since for this experiment the training data is uniformly sampled from the entire image (unlike Fig. 9c) the obtained accuracies are higher than those reported in Table V. Again, the results show that SCDL performs better for urban scenes, even when the training data is as low as 1%.

The Pavia Center image consists of 1096×492 pixels in 102 spectral bands, after 13 noisy bands are removed. Table IV shows the 9 ground-truth classes and test and train sets of the Pavia Center image. The classification results may be seen in Table VII. Similar to the previous image, SCDL obtains the best results, and CSVM and CKSVM perform alike. The previous two images also show the significance of second order moments for HSI classification in urban areas where the classes are usually scattered small regions in the image.

V. CONCLUSION

In this paper, we have investigated dictionary learning algorithms based on models of hyperspectral data for HSI classification. The fundamental idea of the models is to

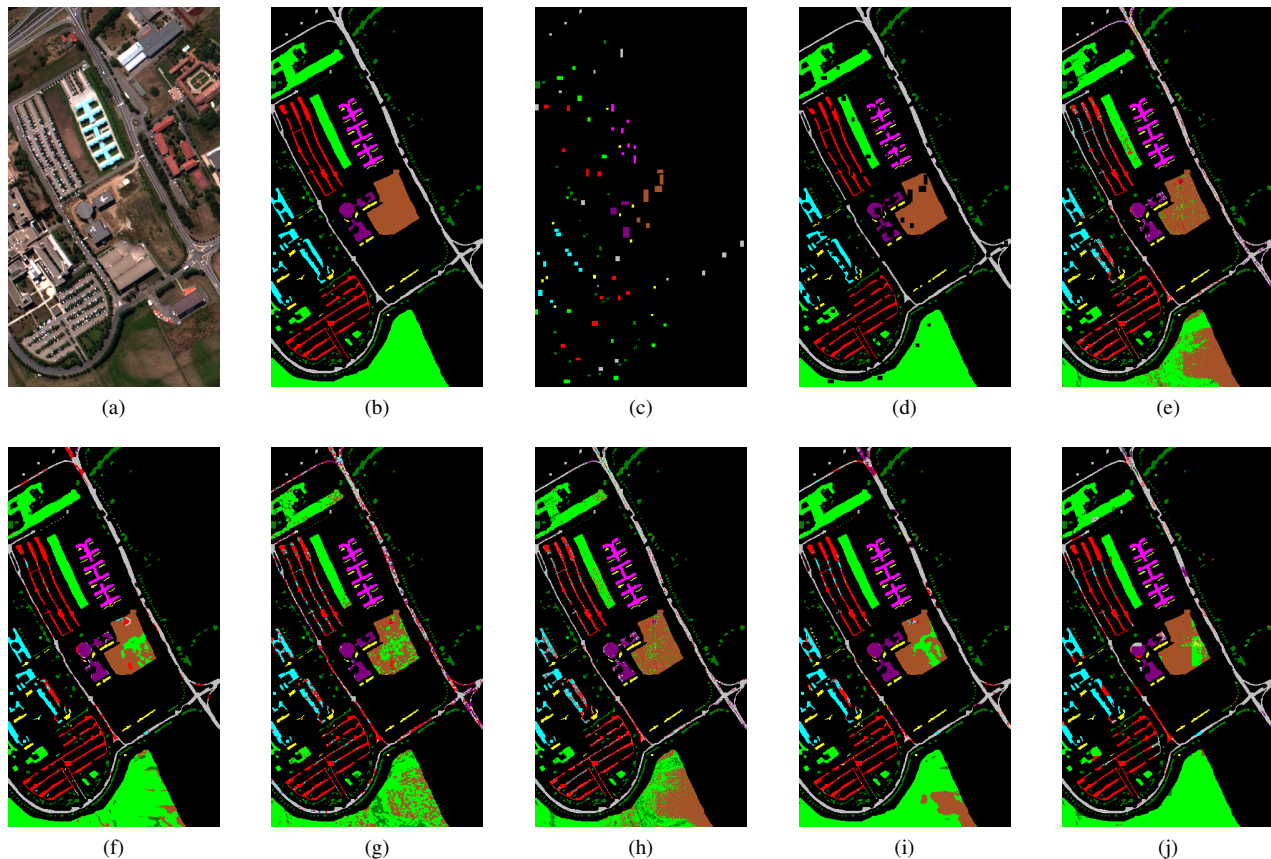


Fig. 9. University of Pavia image. (a) Three-band color composite (bands 50, 27, and 17). (b) Ground-truth. (c) Training data. (d) Test data. Classification maps obtained by (e) SVM, (f) CSVM $_{\mu, \sigma}$, (g) SOMP, (h) SDL, (i) CDL $_{\mu, \sigma}$, and (j) SCDL colored according to Table IV.

TABLE V
CLASSIFICATION ACCURACY (%) ON THE UNIVERSITY OF PAVIA TEST SET FOR DIFFERENT CLASSIFIERS

Class	SVM	CSVM		CK SVM		SOMP	SDL	CDL		SCDL
	-	μ	μ, σ	μ	μ, σ	-	-	μ	μ, σ	-
1	79.54	75.63	88.02	75.63	88.02	50.57	83.52	80.60	87.21	81.87
2	66.23	76.44	92.19	76.44	92.19	71.68	63.36	76.44	86.79	96.48
3	73.55	81.60	80.66	81.60	80.66	73.77	66.73	76.54	75.27	83.36
4	93.68	92.26	99.46	96.26	99.46	96.94	96.36	85.24	92.02	95.47
5	99.82	99.37	75.31	99.37	75.31	99.91	99.62	98.37	98.15	99.82
6	91.86	87.16	85.12	87.16	85.12	64.72	88.11	93.48	71.96	81.21
7	85.83	81.14	94.62	81.14	94.62	95.41	80.92	92.78	92.46	74.11
8	82.82	93.10	95.47	93.10	95.47	83.32	77.19	82.93	88.83	85.91
9	84.91	92.20	95.47	92.20	95.47	94.21	93.53	95.90	99.66	96.60
OA	76.77	81.68	89.74	81.68	89.74	72.29	75.12	81.63	85.90	90.42
AA	84.25	86.99	89.78	86.99	89.78	81.17	83.26	86.92	88.04	88.31
κ	0.711	0.770	0.863	0.770	0.863	0.652	0.693	0.768	0.815	0.870

TABLE VI
CLASSIFICATION ACCURACY (%) ON THE UNIVERSITY OF PAVIA DATASET WITH DIFFERENT NUMBER OF TRAINING DATA

Train	CSVM $_{\mu}$	SOMP	CDL $_{\mu}$	SCDL
1%	93.40 \pm 0.99	78.19 \pm 1.75	93.84 \pm 0.55	94.19 \pm 0.89
2%	95.60 \pm 0.34	82.93 \pm 0.37	95.61 \pm 0.69	96.59 \pm 0.47
4.5%	97.65 \pm 0.30	89.65 \pm 0.55	98.10 \pm 0.22	98.22 \pm 0.29
9%	98.40 \pm 0.14	94.59 \pm 0.30	99.09 \pm 0.09	98.97 \pm 0.10

represent a hyperspectral sample with a linear combination of a few basic elements learned from the data. The spectral samples are classified using a linear SVM trained on the coefficients of this linear combination, known as the sparse representation.

The models were also analyzed from a probabilistic viewpoint. The algorithms were used to exploit either one or both spectral and contextual information for HSI classification. Experiments on real HSI data confirmed the effectiveness of the models for HSI classification.

Many directions of future research are possible. The simple linear SVM yields accurate results, but takes little advantage of the sparsity of the representations. Also, we have observed that the sparse representations of CDL and SCDL are linear separable. Testing the models in conjunction with other classifiers might help us better exploit this potential. There exists a line of supervised dictionary learning algorithms

TABLE VII
CLASSIFICATION ACCURACY (%) ON THE PAVIA CENTER TEST SET FOR DIFFERENT CLASSIFIERS

Class	SVM	CSVM		CK SVM		SOMP	SDL	CDL		SCDL
	-	μ	μ, σ	μ	μ, σ	-	-	μ	μ, σ	-
1	96.40	96.58	96.96	96.58	96.96	97.36	99.41	97.82	99.88	99.40
2	89.64	91.46	94.51	91.46	94.51	83.84	92.54	90.84	94.82	93.19
3	95.16	97.34	97.15	97.34	97.15	95.78	96.02	98.46	97.69	97.49
4	82.60	94.90	99.04	94.90	99.04	70.10	80.62	98.94	94.78	98.32
5	92.27	98.13	94.47	98.13	94.47	96.04	91.19	96.84	92.96	99.27
6	89.17	93.01	92.24	93.01	92.24	77.37	94.99	96.38	98.81	95.45
7	93.50	96.70	93.09	96.70	93.09	92.17	93.15	92.07	86.46	95.77
8	99.00	99.97	99.72	99.97	99.72	98.17	99.59	96.36	98.65	99.59
9	96.19	97.01	92.18	97.01	92.18	94.77	100	97.14	98.53	100
OA	94.87	96.23	96.11	96.23	96.11	94.22	97.78	96.85	98.02	98.47
AA	92.66	96.12	95.48	96.12	94.65	89.51	94.64	96.09	95.84	97.61
κ	0.911	0.934	0.932	0.934	0.932	0.895	0.960	0.945	0.964	0.972

[9], [10] which take advantage of the labels of the training instances to learn the sparse representations in a discriminative manner. To pursue this path we will need to deal with their expensive computation cost. We are also interested in testing the models for semisupervised classification of hyperspectral images, for which transductive SVMs [38] seem to be a plausible choice. Regarding issues other than classification, it would be appealing to define the contextual groups using a smarter algorithm that takes advantage of both spectral and contextual characteristics of HSI.

ACKNOWLEDGMENT

The authors would like to thank the University of Pavia and Prof. Paolo Gamba for kindly providing the ROSIS images of University of Pavia and Center of Pavia and Prof. Landgrebe for the AVIRIS data. Finally, we would also like to thank Dr. Camps-Valls of the University of Valencia, Spain, for helpful discussions regarding the composite kernel SVM.

REFERENCES

- [1] I. Tosić and P. Frossard, "Dictionary learning," *IEEE Signal Process. Mag.*, vol. 28, no. 2, pp. 27–38, Mar. 2011.
- [2] R. Baraniuk, V. Cevher, and M. Wakin, "Low-dimensional models for dimensionality reduction and signal recovery: A geometric perspective," *Proceedings of the IEEE*, vol. 98, no. 6, pp. 959–971, June 2010.
- [3] B. Olshausen and D. Field, "Sparse coding with an overcomplete basis set: A strategy employed by v1?" *Vision research*, vol. 37, no. 23, pp. 3311–3325, 1997.
- [4] M. Aharon, M. Elad, and A. Bruckstein, "K-svd: An algorithm for designing overcomplete dictionaries for sparse representation," *IEEE Trans. Signal Process.*, vol. 54, no. 11, pp. 4311–4322, 2006.
- [5] M. Elad and M. Aharon, "Image denoising via sparse and redundant representations over learned dictionaries," *IEEE Trans. Image Process.*, vol. 15, no. 12, pp. 3736–3745, Dec. 2006.
- [6] J. Yang, K. Yu, Y. Gong, and T. Huang, "Linear spatial pyramid matching using sparse coding for image classification," in *Proc. IEEE Computer Society Conference on Computer Vision and Pattern Recognition Workshops, (CVPR Workshops '09)*, 2009, pp. 1794–1801.
- [7] X. Zhou, K. Yu, T. Zhang, and T. Huang, "Image classification using super-vector coding of local image descriptors," in *Proc. European Conference on Computer Vision (ECCV'10)*, vol. 5. Springer, 2010, pp. 141–154.
- [8] B. J. Culpepper, J. Sohl-Dickstein, and B. Olshausen, "Building a better probabilistic model of images by factorization," in *Proc. IEEE International Conference on Computer Vision (ICCV'11)*, 2011, pp. 2011–2017.
- [9] Q. Zhang and B. Li, "Discriminative k-svd for dictionary learning in face recognition," in *Proc. IEEE Computer Society Conference on Computer Vision and Pattern Recognition (CVPR'10)*, 2010, pp. 2691–2698.
- [10] J. Mairal, F. Bach, and J. Ponce, "Task-driven dictionary learning," *IEEE Trans. Pattern Anal. Mach. Intell.*, vol. 34, no. 4, pp. 791–804, 2012.
- [11] I. Ramirez, P. Sprechmann, and G. Sapiro, "Classification and clustering via dictionary learning with structured incoherence and shared features," in *Proc. IEEE Computer Society Conference on Computer Vision and Pattern Recognition (CVPR'10)*, 2010, pp. 3501–3508.
- [12] E. Elhamifar and R. Vidal, "Sparse manifold clustering and embedding," in *Proc. 25th Annual Conference on Neural Information Processing Systems (NIPS'11)*, vol. 24, 2011, pp. 55–63.
- [13] A. Plaza, J. A. Benediktsson, J. W. Boardman, J. Brazile, L. Bruzzone, G. Camps-Valls, J. Chanussot, M. Fauvel, P. Gamba, A. Gualtieri, M. Marconcini, J. C. Tilton, and G. Trianni, "Recent advances in techniques for hyperspectral image processing," *Remote Sensing of Environment*, vol. 113, Supplement 1, no. 0, pp. S110–S122, 2009.
- [14] A. Bannari, A. Pacheco, K. Staenz, H. McNairn, and K. Omari, "Estimating and mapping crop residues cover on agricultural lands using hyperspectral and ikonos data," *Remote Sensing of Environment*, vol. 104, no. 4, pp. 447–459, 2006.
- [15] A. Larsole and H. H. Muhammed, "Measuring crop status using multivariate analysis of hyperspectral field reflectance with application to disease severity and plant density," *Precision Agriculture*, vol. 8, pp. 37–47, 2007.
- [16] A. Banerjee, P. Burlina, and C. Diehl, "A support vector method for anomaly detection in hyperspectral imagery," *IEEE Trans. Geosci. Remote Sens.*, vol. 44, no. 8, pp. 2282–2291, Aug. 2006.
- [17] M. Eismann, A. Stocker, and N. Nasrabadi, "Automated hyperspectral cueing for civilian search and rescue," *Proceedings of the IEEE*, vol. 97, no. 6, pp. 1031–1055, Jun. 2009.
- [18] R. L. Lawrence, S. D. Wood, and R. L. Sheley, "Mapping invasive plants using hyperspectral imagery and breiman cutler classifications (randomforest)," *Remote Sensing of Environment*, vol. 100, no. 3, pp. 356–362, 2006.
- [19] R. Zomer, A. Trabucco, and S. Ustin, "Building spectral libraries for wetlands land cover classification and hyperspectral remote sensing," *Journal of Environmental Management*, vol. 90, no. 7, pp. 2170–2177, 2009.
- [20] C. Gomez, H. L. Borgne, P. Allemand, C. Delacourt, and P. Ledru, "N-FindR method versus independent component analysis for lithological identification in hyperspectral imagery," *Int. J. Remote Sens.*, vol. 28, no. 23, pp. 5315–5338, Jan. 2007.
- [21] J. M. Bioucas-Dias, A. Plaza, N. Dobigeon, M. P. Q. Du, P. Gader, and J. Chanussot, "Hyperspectral unmixing overview: Geometrical, statistical, and sparse regression-based approaches," *IEEE J. Sel. Topics Topics Appl. Earth Observ.*, vol. 5, no. 2, pp. 354–379, 2012.
- [22] M. D. Iordache, J. M. Bioucas-Dias, and A. Plaza, "Sparse unmixing of hyperspectral data," *IEEE Trans. Geosci. Remote Sens.*, vol. 49, no. 6, pp. 2014–2039, 2011.
- [23] —, "Collaborative sparse unmixing of hyperspectral data," *IEEE Geosci. Remote Sens. Lett.*, pp. 7488–7491, 2012.
- [24] —, "Hyperspectral unmixing with sparse group lasso," in *Proc. IEEE International Geoscience and Remote Sensing Symposium (IGARSS'11)*, 2011, pp. 3586–3589.
- [25] —, "Total variation spatial regularization for sparse hyperspectral unmixing," *IEEE Trans. Geosci. Remote Sens.*, vol. 50, no. 11, pp. 4484–4502, 2012.
- [26] A. Bateson and B. Curtiss, "A method for manual endmember selection

- and spectral unmixing,” *Remote Sensing of Environment*, vol. 55, no. 3, pp. 229–243, 1996.
- [27] A. S. Charles, B. A. Olshausen, and C. J. Rozell, “Learning sparse codes for hyperspectral imagery,” *IEEE J. Sel. Topics Signal Process.*, vol. 5, no. 5, pp. 963–978, 2011.
- [28] A. Castrodad, X. Zhengming, J. B. Greer, E. Bosch, L. Carin, and G. Sapiro, “Learning discriminative sparse representations for modeling, source separation, and mapping of hyperspectral imagery,” *IEEE Trans. Geosci. Remote Sens.*, vol. 49, no. 11, pp. 4263–4281, 2011.
- [29] J. Greer, “Sparse demixing of hyperspectral images,” *IEEE Trans. Image Process.*, vol. 21, no. 1, pp. 219–228, 2012.
- [30] J. Benediktsson, J. Palmason, and J. Sveinsson, “Classification of hyperspectral data from urban areas based on extended morphological profiles,” *IEEE Trans. Geosci. Remote Sens.*, vol. 43, no. 3, pp. 480–491, Mar. 2005.
- [31] G. Camps-Valls, L. Gómez-Chova, J. Calpe-Maravilla, F. Soria-Olivas, J. Martín-Guerrero, and J. Moreno, “Support vector machines for crop classification using hyperspectral data,” *Pattern recognition and image analysis*, vol. 2652, pp. 134–141, 2003.
- [32] D. Landgrebe, *Signal Theory Methods in Multispectral Remote Sensing*. New York: Wiley, 2003.
- [33] P. Goel, S. Prasher, R. Patel, J. Landry, R. Bonnell, and A. Viau, “Classification of hyperspectral data by decision trees and artificial neural networks to identify weed stress and nitrogen status of corn,” *Computers and Electronics in Agriculture*, vol. 39, no. 2, pp. 67–93, 2003.
- [34] H. Yang, “A back-propagation neural network for mineralogical mapping from aviris data,” *International Journal of Remote Sensing*, vol. 20, no. 1, pp. 97–110, 1999.
- [35] A. Gualtieri, S. Chettri, R. Crompt, and L. Johnson, “Support vector machine classifiers as applied to aviris data,” in *Proceedings of The 1999 Airborne Geoscience Workshop*, Feb. 1999.
- [36] F. Melgani and L. Bruzzone, “Classification of hyperspectral remote sensing images with support vector machines,” *IEEE Trans. Geosci. Remote Sens.*, vol. 42, no. 8, pp. 1778–1790, Aug. 2004.
- [37] G. Camps-Valls, T. B. Marsheva, and D. Zhou, “Semi-supervised graph-based hyperspectral image classification,” *IEEE Trans. Geosci. Remote Sens.*, vol. 45, no. 10, pp. 3044–3054, Oct. 2007.
- [38] L. Bruzzone, M. Chi, and M. Marconcini, “A novel transductive svm for semisupervised classification of remote-sensing images,” *IEEE Trans. Geosci. Remote Sens.*, vol. 44, no. 11, pp. 3363–3373, Nov. 2006.
- [39] G. Camps-Valls, L. Gomez-Chova, J. Munoz-Mari, J. Vila-Frances, and J. Calpe-Maravilla, “Composite kernels for hyperspectral image classification,” *IEEE Geosci. Remote Sens. Lett.*, vol. 3, no. 1, pp. 93–97, Jan. 2006.
- [40] G. Camps-Valls, N. Shervashidze, and K. M. Borgwardt, “Spatio-spectral remote sensing image classification with graph kernels,” *IEEE Geosci. Remote Sens. Lett.*, vol. 7, no. 4, pp. 741–745, 2010.
- [41] Y. Chen, N. Nasrabadi, and T. Tran, “Hyperspectral image classification using dictionary-based sparse representation,” *IEEE Trans. Geosci. Remote Sens.*, vol. 49, no. 10, pp. 3973–3985, Oct. 2011.
- [42] S. Cotter, B. Rao, K. Engan, and K. Kreutz-Delgado, “Sparse solutions to linear inverse problems with multiple measurement vectors,” *IEEE Trans. Signal Process.*, vol. 53, no. 7, pp. 2477–2488, Jul. 2005.
- [43] J. Tropp, “Algorithms for simultaneous sparse approximation. part ii: Convex relaxation,” *Signal Processing*, vol. 86, no. 3, pp. 589–602, 2006.
- [44] R. Tibshirani, “Regression shrinkage and selection via the lasso,” *Journal of the Royal Statistical Society. Series B (Methodological)*, vol. 58, no. 1, pp. 267–288, 1996.
- [45] K. Kreutz-Delgado, J. Murray, B. Rao, K. Engan, T. Lee, and T. Sejnowski, “Dictionary learning algorithms for sparse representation,” *Neural computation*, vol. 15, no. 2, pp. 349–396, 2003.
- [46] M. Osborne, B. Presnell, and B. Turlach, “A new approach to variable selection in least squares problems,” *IMA journal of numerical analysis*, vol. 20, no. 3, pp. 389–403, 2000.
- [47] B. Efron, T. Hastie, I. Johnstone, R. Tibshirani, H. Ishwaran, K. Knight, J. Loubes, P. Massart, D. Madigan, G. Ridgeway, S. Rosset, J. Zhu, R. Stine, B. Turlach, and S. Weisberg, “Least angle regression,” *Annals of Statistics*, vol. 32, no. 2, pp. 407–499, 2004.
- [48] H. Lee, A. Battle, R. Raina, and A. Y. Ng, “Efficient sparse coding algorithms,” in *Proc. Conference on Neural Information Processing Systems (NIPS) ’07*, 2007, pp. 801–808.
- [49] J. Mairal, F. Bach, J. Ponce, and G. Sapiro, “Online learning for matrix factorization and sparse coding,” *The Journal of Machine Learning Research*, vol. 11, pp. 19–60, Mar. 2010.
- [50] J. Mairal. Spams: Sparse modeling software. [Online]. Available: <http://spams-devel.gforge.inria.fr>
- [51] K. Engan, S. Aase, and J. H. Husoy, “Method of optimal directions for frame design,” in *Proc. IEEE International Conference on Acoustics, Speech, and Signal Processing (ICASSP) ’99*, vol. 5, 1999, pp. 2443–2446.
- [52] A. F. T. Martins, N. A. Smith, P. M. Q. Aguiar, and M. A. T. Figueiredo, “Structured sparsity in structured prediction,” in *Proceedings of the Conference on Empirical Methods in Natural Language Processing (EMNLP ’11)*. Stroudsburg, PA, USA: Association for Computational Linguistics, 2011, pp. 1500–1511.
- [53] D. Malioutov, M. Cetin, and A. Willsky, “A sparse signal reconstruction perspective for source localization with sensor arrays,” *IEEE Trans. Signal Process.*, vol. 53, no. 8, pp. 3010–3022, Aug. 2005.
- [54] H. Lu, X. Long, and J. Lv, “A fast algorithm for recovery of jointly sparse vectors based on the alternating direction methods,” *Journal of Machine Learning Research*, vol. 15, pp. 461–469, 2011.
- [55] A. Rakotomamonjy, “Surveying and comparing simultaneous sparse approximation (or group-lasso) algorithms,” *Signal processing*, vol. 91, no. 7, pp. 1505–1526, 2011.
- [56] J. Yang and Y. Zhang, “Alternating direction algorithms for ℓ_1 -problems in compressive sensing,” *SIAM journal on scientific computing*, vol. 33, no. 1, pp. 250–278, 2011.
- [57] S. R. Searle, *Matrix Algebra Useful for Statistics*. John Wiley and Sons, Oct. 1982.
- [58] Y. Tarabalka, J. Benediktsson, and J. Chanussot, “Spectral-spatial classification of hyperspectral imagery based on partitioning clustering techniques,” *IEEE Trans. Geosci. Remote Sens.*, vol. 47, no. 8, pp. 2973–2987, Aug. 2009.
- [59] C. Chih-Chung and L. Chih-Jen, “LIBSVM: A library for support vector machines,” *ACM Transactions on Intelligent Systems and Technology*, vol. 2, pp. 27:1–27:27, 2011, software available at <http://www.csie.ntu.edu.tw/~cjlin/libsvm>.
- [60] AVIRIS NW Indiana’s Indian Pines 1992 data set. [Online]. Available: <https://engineering.purdue.edu/~biehl/MultiSpec/hyperspectral.html>
- [61] J. A. Richards, *Remote Sensing Digital Image Analysis: An Introduction*, 5th ed. New York: Springer-Verlag, 2013.
- [62] The Benefits of the 8-Spectral Bands of Worldview-2, Mar 2010. [Online]. Available: http://www.digitalglobe.com/downloads/WorldView-2_8-Band_Applications_Whitepaper.pdf



Ali Soltani-Farani received his M.Sc. in Computer Architecture from Sharif University of Technology, Tehran, Iran, in 2010 and a B.Sc. in Hardware Engineering from the same university in 2008. He is currently working toward the Ph.D. degree in the Department of Computer Engineering at Sharif University of Technology.

From 2012 he works as a Technical Consultant at the Value Added Services Laboratory (VASL) and is an adjunct lecturer at Sharif University of Technology, Tehran, Iran. His current research interests include structured sparse representations, dictionary learning, and their application to signal and image processing.



Hamid R. Rabiee (SM'07) received his B.S. (1987) and M.S. (1989) degrees (with great distinction) in Electrical Engineering from CSULB, USA, his EEE in Electrical and Computer Engineering from USC, USA, and his Ph.D. (1996) in Electrical and Computer Engineering from Purdue University, West Lafayette, USA.

From 1993 to 1996 he was a Member of Technical Staff at AT&T Bell Laboratories. From 1996 to 1999 he worked as a Senior Software Engineer at Intel Corporation. He was also with PSU, OGI, and OSU Universities as an adjunct professor of Electrical and Computer Engineering from 1996 to 2000. Since September 2000, he has joined Sharif University of Technology (SUT), Tehran, Iran. He is the founder of Sharif University Advanced Information and Communication Technology Research Center (AICT), Advanced Technologies Incubator (SATI), Digital Media Laboratory (DML) and Mobile Value Added Services Laboratory (VASL). He is currently a Professor of Computer Engineering at Sharif University of Technology and the Director of AICT, DML and VASL. He has been the initiator and director of national and international level projects in the context of UNDP International Open Source Network (IOSN) and Iran National ICT Development Plan.

Prof. Rabiee has received numerous awards and honors for his industrial, scientific and academic contributions. He has acted as chairman in a number of national and international conferences, and holds three patents.



Seyyed Abbas Hosseini received his B.Sc. in Software Engineering from Sharif University of Technology, Tehran, Iran, in 2012 and is currently working towards his M.Sc. degree in the Department of Computer Engineering at Sharif University of Technology.

His current research interests include the application of dictionary learning and metric learning to image classification.